A GEOMETRIC SIMULATOR FOR THE HYPERSPECTRAL MISSION ENMAP

P. Schwind, R. Müller, G. Palubinskas, T. Storch, C. Makasy

German Aerospace Center (DLR), Remote Sensing Technology Institute, D-82234 Wessling, Germany
email: {Peter.Schwind, Rupert.Mueller, Gintautas.Palubinskas, Tobias.Storch, Christine.Makasy}@dlr.de

Commission I/4

KEY WORDS: geometric simulation, geometric correction, EnMAP

ABSTRACT:

The hyperspectral satellite EnMAP (Environmental Mapping and Analysis Program) is scheduled to launch in 2014. It is a joint project by the GFZ (Deutsches GeoForschungsZentrum), the DLR (German Aerospace Center), Kayser-Threde and OHB-System. Apart from the project management, the DLR is responsible for the development of the ground segment for EnMAP. One of the key steps of the developed processing chain is the geometric correction of the EnMAP data. As EnMAP uses an in-field separation design, corresponding areas on the Earth are imaged with a time delay of approximately 88 ms. This in combination with attitude controller errors, board instrument vibrations as well as external effects, such as the rotation of the Earth, leads to co-registration inaccuracies between the VNIR and SWIR data. As it is not possible to correct this error by imager design, it has to be corrected after the image acquisition during the geometric correction step. To be able to test and validate if the desired co-registration accuracy of 0.2 pixels can be achieved using the developed geometric processor, a geometric simulator was implemented. The simulator design as well as the co-registration results achieved by the geometric correction are discussed in this paper.

1 INTRODUCTION

The Applied Remote Sensing Cluster (CAF) at DLR has long lasting experiences with the processing of high-resolution panchromatic and multispectral airborne and spaceborne acquired images. Within the future hyperspectral satellite mission EnMAP (Environmental Mapping and Analysis Program), DLR is responsible for the establishment of the ground segment (Storch et al., 2010, Müller et al., 2009). This includes the mission operations system, the payload ground system together with the processor, calibration and product quality control responsible for instrument in-flight calibration as well as the establishment of an automatic processing chain.

The EnMAP bus carries two imaging spectrometers, a CMOS focal plane array for the VNIR (visible and near infrared) spectral range and a MCT detector array for the SWIR (short-wavelength infrared) spectral range (Storch et al., 2008). The used in-field separation design, realized by a double slit, leads to an acquisition delay of 88 ms for corresponding areas on the Earth surface. This, in combination with attitude controller errors, board instrument vibrations as well as external effects, such as the rotation of the Earth, leads to co-registration inaccuracies between the VNIR and SWIR data. As the required geometric co-registration accuracy of 0.2 pixels between the VNIR and SWIR channels cannot be achieved by imager design alone, post-acquisition processing of the data is necessary.

Since no EnMAP data is available before the satellite launch, a geometric simulator was developed for testing and validation purposes. The basic idea of this simulator is to generate artificial orbit and attitude parameters of the EnMAP satellite and employ these to virtually acquire EnMAP scenery using a geocoded image as reference. The attitude and orbit metadata generated during this step are artificially flawed with the expected knowledge errors to evaluate if they can be reconstructed with sufficient accuracy for the orthorectification. Finally, the generated VNIR and SWIR images can be orthorectified using the algorithms implemented for the future EnMAP processor and their relative accuracy is measured. The functionality of the geometric simulator as well as the results achieved are discussed in this paper.

It should be noted that an EnMAP simulator, including a geometric module, was also presented in (Guanter et al., 2009). However, the geometric part of that simulator is only explained generally with a reference to a future paper with more details which had not been published at the time of writing of this work. For the interested reader other examples of geometric satellite simulation can be found in (Riihimäki and Ylén, 2005, Li et al., 2000).

2 GEOMETRIC CORRECTION

As the scope of this paper is focused on the geometric correction of EnMAP data, a short summary of the coregistration problem and the geometric correction is given hereafter.

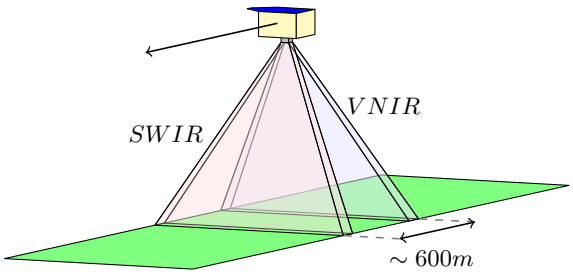

Figure 1: Acquisition difference between SWIR and VNIR detectors.

2.1 Coregistration problem

The in-field separation design used by EnMAP to acquire the VNIR and SWIR channels leads to an acquisition delay of 88 ms ($\approx$ 600 m) on the ground (see Figure 1). As the target coregistration accuracy for the EnMAP VNIR and SWIR channels is to be better than 0.2 pixels, the coregistration error resulting from imager design has to be corrected after the image acquisition. Using the expected error of the attitude controller as well as expected

minor instrument vibrations, it is possible to compute a first estimate of the coregistration error of the VNIR and SWIR sensors. In Figure 2 the variation in pointing for a time frame of 88 ms has been plotted. The maximum variation of 0.00071° (≈ 8.13 m on the ground) shows that the co-registration accuracy of 0.2 pixels cannot be met without a geometric correction of the images.

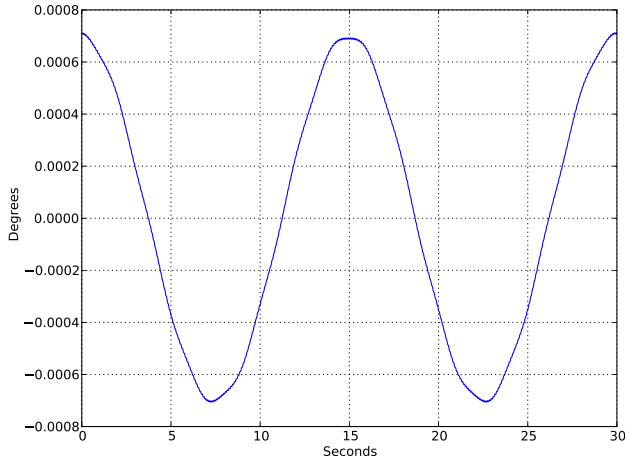

Figure 2: Variation of pointing in a time frame of 88 ms (max=0.00071° ≈ 8.13 m on the ground)

The entire geometric correction of the coregistration error is further complicated by the fact that the AOCS (Attitude & Orbit Control Subsystem) data of the satellite is only available with a frequency of 1 Hz. This means the AOCS data will have to be either interpolated or approximated to obtain the the missing parameters for the correction of each image line. In addition to that the already incomplete AOCS data is flawed by instrument knowledge errors, which unfortunately impair these interpolation/approximation results.

2.2 Orthorectification

For the orthorectification of EnMAP images the DLR in-house generic orthorectification processor ORTHO (Müller et al., 2005) is used, processing the VNIR and SWIR images seperately. This processor employs direct georeferencing (Müller et al., 2002), an algorithm based on the collinearity concept, to establish a relation between the mapped object points and their corresponding image coordinates. The whole orthorectification process starts with the establishment of the Line-of-Sight (LoS) model, which uses the measurements of the precision orbit data (state vectors, attitude, timing information), the sensor mounting and the sensor model. Since the sensor model used for direct georeferencing was also used for the creation of the simulated images it is explained in more detail hereafter.

An overview of the geometric model used for direct georeferencing can be seen in Figure 3. The position of the sensor relative to Earth is given in Earth-Centred Earth-Fixed (ECEF) coordinates r_{Sensor}^{ECEF}. The attitude $R_{Sensor}^{Orbital}$ of the sensor is given in the orbital coordinate system, which is centred at the barycentre of the satellite and aligned to the orbit center and the orbit plane. For the interior orientation r_{Object}^{Sensor} an idealized pushbroom sensor model was used. Using an ellipsoid as the assumed Earth surface the scale factor λ can be computed. Based on the collinearity concept, the vector to the object point on the surface of the Earth r_{Object}^{ECEF} can thus be determined by the equation

$$r_{Object}^{ECEF} = r_{Sensor}^{ECEF} + \lambda \cdot R_{Orbital}^{ECEF} \cdot R_{Sensor}^{Orbital} \cdot r_{Object}^{Sensor} \quad (1)$$

where the rotation matrix $R_{Orbital}^{ECEF}$ denotes a change of basis from the Orbital to the ECEF coordinate system. The position r_{Sensor}^{ECEF} and the attitude $R_{Sensor}^{Orbital}$ have to be specified for each line of a scene, while the interior orientation r_{Object}^{Sensor} can be computed from given sensor parameters. The scale factor λ can then be computed using these parameters by intersecting each pixel view vector with the Earth ellipsoid. For a more detailed description of the sensor model refer to (Müller et al., 2002, Müller et al., 2005).

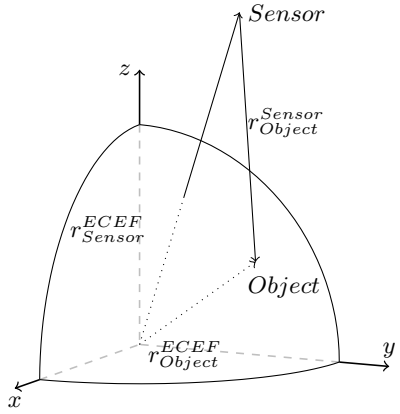

Figure 3: Sensor model used for direct georeferencing

3 GEOMETRIC SIMULATOR

Several processing steps are necessary to create a simulated EnMAP scene with realistic geometric properties. First the used reference scene is resampled to a spatial resolution of 30 m using a Gaussian filter. In the next step artificial position and attitude data are generated and the expected position and attitude controller deviations are added. Using these simulated AOCS data the reference images are scanned and the simulated EnMAP imagery is created. Before the AOCS data is saved for the latter orthorectification it is further altered with the expected attitude and position knowledge errors. Next, the erroneous AOCS data is corrected using curve fitting and interpolation, so the finally reconstructed parameters can be used to orthorectify the image. A more detailed explanation of the entire process is given in the following.

3.1 Resampling to EnMAP resolution

To avoid aliasing effects by an image subsampling, a low pass filter is applied to the reference image. Let's assume that an input image I has a resolution ρ_{high}. The aim is from a high resolution image I to produce an image O with a reduced resolution ρ_{low} satisfying a condition $\rho_{low} > \rho_{high}$. From a signal processing view a low pass filter with given band pass characteristics is usually constructed in the spectral domain. For example the Gaussian filter is expressed by the following formula

$$H(f) = e^{-\frac{1}{2}(\frac{f}{f_c})^2} \quad (2)$$

where f is a frequency, f_c is a cut-off frequency of a signal spectrum and is defined as $f_c = f_{max} \cdot r$ where f_{max} is a maximal frequency and $r = \rho_{high}/\rho_{low}$. The desired low pass filter in an image domain is then an inverse Fourier transform of the filter H: $h = FFT^{-1}(H)$. Finally, a filtered image $O = I * h$ can be simply subsampled to the required resolution.

3.2 Image generation

To simulate the image acquisition, artificial satellite position and attitude are used in combination with the sensor model introduced in Section 2.2, allowing to obtain exact geocoordinates for each pixel of an image. Using a geocoded image the corresponding pixel values for each geocoordinate can be extracted.

For the simulation the position r_{Sensor}^{ECEF} (see Equation 1) is calculated using the expected orbit parameters (see Table 1), while the attitude $R_{Sensor}^{Orbital}$ is adjusted to Nadir view. The artificial AOCS data meant for the future orthorectification of the images is generated with a frequency of 1 Hz using the same values with added randomized errors, simulating measurement uncertainties. The attitude controller as well as the position knowledge error are both expected to have a normal distributed error with a standard deviation of 0.0037° (total error for pitch and roll) and 17.5 m (for each dimension) respectively.

Eccentricity	0.0011353
Semimajor axis	7021.881342 km
Inclination	97.9617°
Longitude of the ascending node	86.4684°
Argument of periapsis	250.0823°
True anomaly	109.9183°

Table 1: Expected EnMAP orbit parameters

3.3 Approximation/interpolation of AOCS data

To evaluate if the used fitting function is adequate for the correction of the images, AOCS data with and without the expected deviations is created. Here, detailed information about the approximation and interpolation of erroneous attitude and position data is given.

3.3.1 Attitude To simulate the orthorectification of EnMAP imagery, only the noisy attitude data is used for this step. A sinusoidal curve is fitted to the available attitude measurements using least squares fitting (Levenberg-Marquardt algorithm) to obtain a better approximation of the real attitude deviation. It should be mentioned that even though a sinusoidal curve was assumed here, the really expected attitude deviation for EnMAP will likely be more similar to a sum of sinuses. However it is expected, that out of all error influences on the attitude deviation, the attitude controller error will by far have the biggest impact.

While the recording frequency of the AOCS data has already been specified at 1 Hz, the time interval before and after the scene acquisition for which this data is available has not been established yet. Here, we assumed that AOCS data including attitude measurements would be available 60 seconds before and after the scene acquisition. Naturally a shorter timespan would lead to a less reliable approximation of the real attitude deviation while a longer timespan should improve results.

An example of the approximation of the pointing deviation can be seen in Figure 4. The shown approximated curve (red) has a mean displacement of -0.0004° with a standard deviation of 0.0003° from the real attitude deviation.

3.3.2 Position Like the attitude data, the position measurements are available with a frequency of 1 Hz. However the influence of the orbit position on the coregistration accuracy is negligible compared to the attitude accuracy. That is why the missing position values are obtained by simply applying Lagrange interpolation.

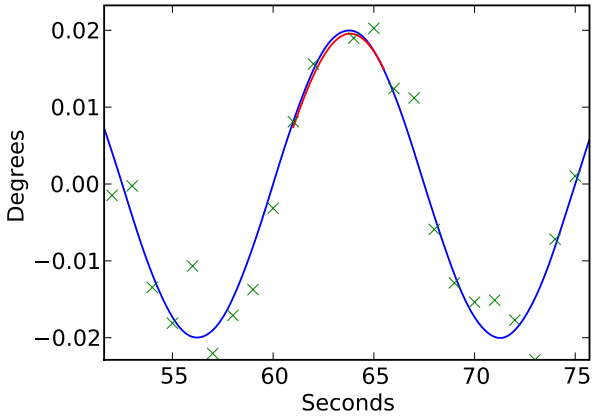

Figure 4: Example of the approximation of the attitude controller deviation. Blue: the real deviation; Green: periodic attitude measurements including pointing knowledge error; Red: Approximated deviation for the duration of an EnMAP scene

4 EVALUATION OF THE COREGISTRATION

After the simulated EnMAP image and appendant AOCS data were created for the VNIR and SWIR channels, the images were orthorectified using the process described in section 2.2. The methodology applied to determine the absolute accuracy of the corrected scenes as well as accuracy relative to each other is explained hereafter, followed by a discussion of the obtained results.

4.1 Methodology

The images were orthorectified once using the AOCS data containing the correct attitude information and once using the data containing the approximated attitude information (see Section 3.3). As using the correct AOCS data for the orthorectification basically corresponds to reversing the creation of the simulated images back to the source image this was an easy way to confirm the correctness of the simulator and to get an estimate of minor error influences on the processed images, such as resampling or rounding errors.

To determine the absolute accuracy of the images, the exact geocoordinates for each pixel of the simulated images are stored during image generation. During orthorectification new geocoordinates are calculated for each of these points. The difference of the original coordinates to the new orthorectified coordinates represents the absolute accuracy for each pixel. As these calculations in vector-space are not subject to image resampling, when using the correct AOCS data this difference shows the errors introduced for example by rounding errors or floating point inaccuracies. Unfortunately this way it is not currently possible to directly calculate the co-registration accuracy between the VNIR and SWIR channels, as the same geocoordinates would have to be selected in the simulated images prior to the orthorectification process. This task is not as trivial as it may seem at first glance, because of the way the simulator works: The recorded geocoordinates are derived from the satellite position and attitude as well as the interior orientation of the scan line elements. Selecting a geocoordinate and finding the subpixel coordinate which it is projected to would basically correspond to an inversion of this simulation process.

The coregistration error between the SWIR and VNIR images was calculated using a more empiric approach. After the orthorectification step the VNIR and SWIR images were matched

using the pyramid based matching algorithm described in (Lehner and Gill, 1992, Kornus et al., 1999). It should be noted that the required matching accuracy of better than 6 m is already getting close to immeasurable in images with a resolution of 30 m. However the used matching process has been shown to have an accuracy of up to 0.1 pixels in (Kornus et al., 1999). In addition to that, the number of matches for the very similar images was always very high ($\sim$ 1000 matches), so that the calculated mean displacement of all matches is assumed to be reliable.

The chosen reference image was an ALOS/PRISM scene (Nadir) of the area around Oberpfaffenhofen, Germany (see Figure 5). A PRISM scene was chosen as it has the scene extent necessary to acquire a complete EnMAP scene (40 km $\times$40 km) as well as a relatively high resolution (2.5 m).

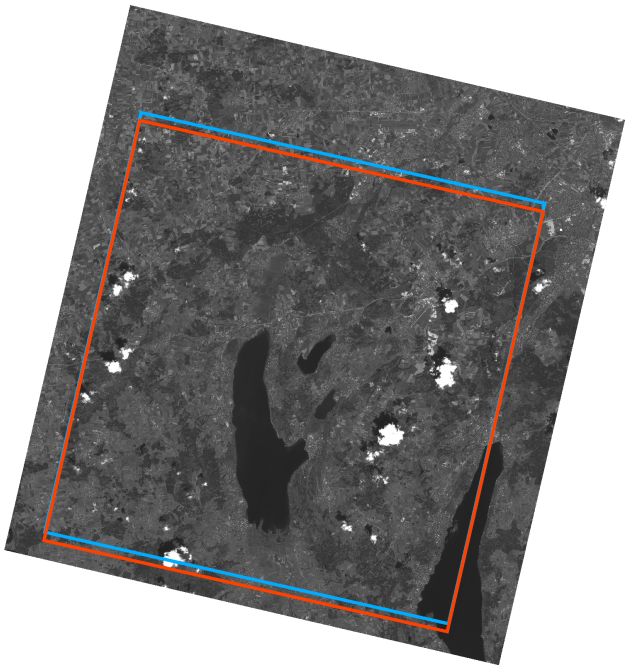

Figure 5: Used reference scene (PRISM) with footprints of simulated VNIR (blue) and SWIR (red) scenes

4.2 Results

For the statistics calculation the entire processing chain was run for a total of 1000 iterations. The results are presented for both the correct AOCS data as well as the data corrected using curve fitting and interpolation (approximated AOCS data).

4.2.1 Absolute accuracy The average absolute accuracy of a total of 1000 processed scenes can be seen in Table 2. The low absolute deviation when using the correct AOCS data (Std.-dev. 0.655 m in x and 0.152 m in y for VNIR) confirms the correctness of the entire simulation process. Small remaining errors probably result from rounding errors and floating point inaccuracies. For the approximated AOCS data the absolute accuracy shows a somewhat deteriorated performance (Std.-dev. 16.296 m in x and 18.761 m in y for VNIR). This results from the position and attitude inaccuracies of the satellite. However, as long as both VNIR and SWIR have a similar absolute accuracy, this does not pose a big problem for their coregistration accuracy. Sample plots showing the absolute accuracy of an equidistant grid of points of a VNIR scene are shown in Figure 6 and 7 for the correct AOCS data and the approximated data respectively (Note the different scales: 1 m vs. 30 m).

VNIR	x	y
Correct AOCS data		
Mean	0.062 m	0.047 m
Std.-dev.	0.655 m	0.152 m
Approximated AOCS data		
Mean	7.252 m	7.076 m
Std.-dev.	16.296 m	18.761 m
SWIR		
Correct AOCS data		
Mean	0.007 m	0.006 m
Std.-dev.	0.654 m	0.152 m
Approximated AOCS data		
Mean	7.251 m	7.075 m
Std.-dev.	16.296 m	18.761 m

Table 2: Absolute accuracy of the corrected VNIR and SWIR images (generated over 1000 iterations).

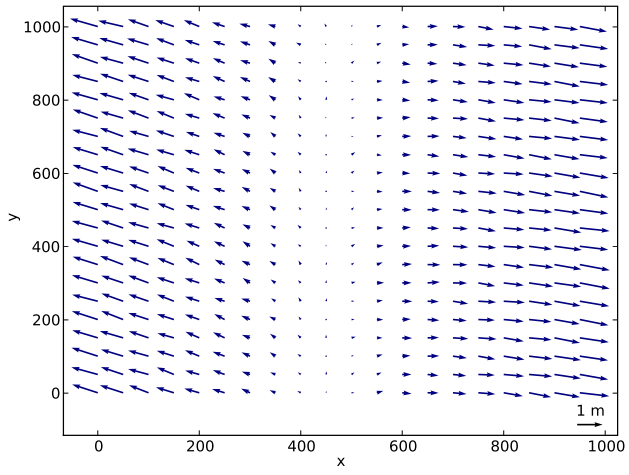

Figure 6: Deviation in meters of the geocoordinates, orthorectified using the correct AOCS data, from their original coordinates.

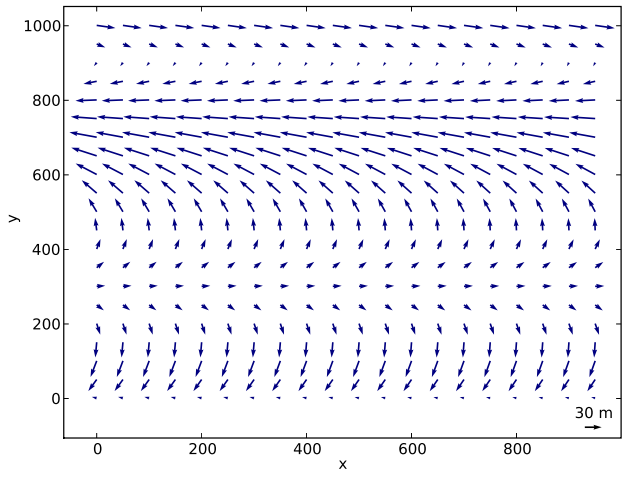

Figure 7: Deviation in meters of the geocoordinates, orthorectified using the approximated AOCS data, from their original coordinates.

4.2.2 Relative accuracy For the matches returned by the pyramid matching the absolute mean displacement as well as the standard deviation was calculated for 1000 iterations (see Table 3). When using the correct AOCS data a mean displacement of

0.739 m in x and 1.403 m in y was determined with a standard deviation of 3.103 m in x and 2.640 m in y respectively. For the AOCS data created using the realistic attitude and position information (approximated AOCS data) an absolute mean displacement of 1.122 m in x and 1.542 m in y was observed with a standard deviation of 3.554 m and 4.321 m in x and y respectively. An example of the displacements of the obtained matches between two VNIR and SWIR scenes can be observed in Figure 8.

	x	y
Correct AOCS data		
Mean	0.739 m	1.403 m
Std.-dev.	3.103 m	2.640 m
Approximated AOCS data		
Mean	1.122 m	1.542 m
Std.-dev.	3.554 m	4.321 m

Table 3: Absolute mean displacement and standard deviation between the matches found in the orthorectified VNIR and SWIR images in meters (generated over 1000 iterations).

It is notable that the absolute accuracy of the correct AOCS data for VNIR and SWIR is better than 1 m (see Table 2), while the standard deviation returned by the pyramid matching is 3.103 m and 2.640 m in x and y respectively (see Table 3). As the relative error between both scenes cannot be higher than the sum of their absolute deviations ($\sim$ 1.5 m in 2 dimensions), the remaining error has to be a result of matching inaccuracies. This also matches up with the specified accuracy of $\sim$ 0.1 pixels ($\approx$ 3 m) of the used matching algorithm. However the fact, that the standard deviation of the data orthorectified using the approximated AOCS data is only slightly worse than that of the correct data (3.554 m and 4.321 m in x and y respectively), suggests that the coregistration accuracy in 2 dimensions averaged over 1000 simulated scenes is better than 3 m.

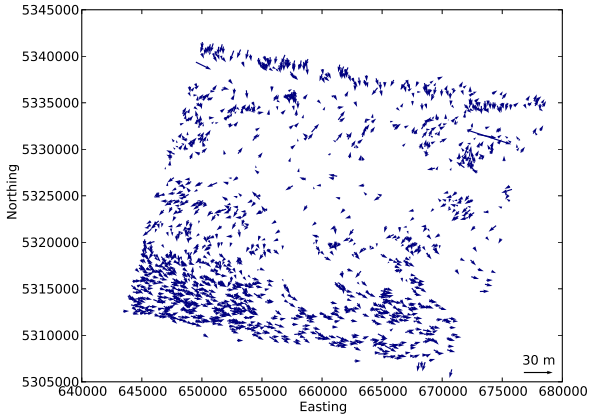

Figure 8: Deviations between the matches found in two VNIR and SWIR scenes orthorectified using the approximated AOCS data.

5 CONCLUSIONS

A geometric simulator for EnMAP was devised and implemented. Based on an idealized sensor model this simulator calculates artificial satellite AOCS data and uses these to scan an existing remote sensing image. A random error corresponding to the expected measuring accuracy of the attitude and position controllers is added to metadata created together with this image. The simulated AOCS data is corrected using curve fitting and interpolation and these parameters are used to orthorectify the simulated scenes.

The evaluation of this process has shown that the required coregistration accuracy of 6 m can be met if AOCS data is improved this way. However the task of measuring the coregistration accuracy in an image with a resolution of 30 m is problematic. It would be more desirable to apply a rigid approach, like the one used to measure the absolute accuracy, to the evaluation of the relative coregistration accuracy.

For the future development of the geometric simulator, there are still several points left for improvement. While the presented evaluation was performed always assuming a Nadir viewing angle, it would also be interesting to evaluate the accuracy for the sidelooking modes. In that context it would also be reasonable to use a digital elevation model to describe the Earth surface instead of the currently used ellipsoid. It would also be desirable to use a reference image with a higher resolution than the used ALOS/PRISM scene. As sensors with higher resolution than ALOS/PRISM usually don't have the scene extent required for a simulated EnMAP scene, a mosaic of high-resolution would be suitable for this purpose. For a more realistic simulation, it would also be necessary to use an interior sensor model fitting more closely to the real model instead of the currently used idealized pushbroom model. At the time of writing however, too many parameters of such a model were still unknown to reasonably implement it. Finally, the model used for the satellite attitude was still somewhat unrealistic as currently the only major influence on these parameters is the attitude controller error. Other relevant factors, such as the heating up of the satellite under sunlight exposure are currently not part of the simulation. This would also influence the approximation of the real attitude deviation, as the currently fitted sinusoidal oscillation might not be sufficient for this task any more. These and other issues will be addressed in the simulator as more details of the satellite design and laboratory instrument measurements become known.

REFERENCES

Guanter, L., Segl, K. and Kaufmann, H., 2009. Simulation of optical remote-sensing scenes with application to the EnMAP hyperspectral mission. Geoscience and Remote Sensing, IEEE Transactions on 47(7), pp. 2340 –2351.

Kornus, W., Lehner, M. and Schroeder, M., 1999. Geometric inflight-calibration by block adjustment using MOMS-2P imagery of three intersecting stereo-strips.

Lehner, M. and Gill, R., 1992. Semi-automatic derivation of digital elevation models from stereoscopic 3-line scanner data. ISPRS 29, B4, pp. 68–75.

Li, R., Zhou, G., Yang, S., Tuell, G., Schmidt, N., and Flower, C., 2000. A study of the potential attainable geometric accuracy of ikonos satellite imagery. In: International Archives of Photogrammetry and Remote Sensing, Vol. 33, B4, p. 587595.

Müller, R., Bachmann, M., Makasy, C., Miguel, A., Müller, A., Neumann, A., Palubinskas, G., Richter, R., Schneider, M., Storch, T., Walzel, T., hermann Kaufmann, Guanter, L. and Segl, K., 2009. EnMAP - the future hyperspectral satellite mission product generation. In: C. Heipke, J. Karsten, S. Müller and U. Sörgel (eds), ISPRS Hannover Workshop 2009, High-Resolution Earth Imaging for Geospatial Information, XXXVIII-1-4-7 / W5, ISPRS.

Müller, R., Lehner, M., Müller, R., Reinartz, P., Schroeder, M. and Vollmer, B., 2002. A program for direct georeferencing of airborne and spaceborne line scanner images. In: Integrating Remote Sensing at the Global, Regional and Local Scale, Denver CO, Nov. 10-15 2002, Vol.XXXIV, Part 1; Commision I, Vol. 1, pp. 148–153.

Müller, R., Lehner, M., Reinartz, P. and Schroeder, M., 2005. Evaluation of spaceborne and airborne line scanner images using a generic ortho image processor. In: C. Heipke, K. Jacobsen and M. Gerke (eds), High Resolution Earth Imaging for Geospatial Information, Hannover, 17.-20. Mai 2005, IAPRS, Vol. XXXVI.

Riihimäki, P. and Ylén, J.-P., 2005. Simulation of spacecraft attitude and orbit dynamics. In: 19th European Conference on Modelling and Simulation.

Storch, T., de Miguel, A., Müller, R., Müller, A., Neumann, A., Walzel, T., Bachmann, M., Palubinskas, G., Lehner, M., Richter, R., Borg, E., Fichtelmann, B., Heege, T., Schroeder, M. and Reinartz, P., 2008. The future spaceborne hyperspectral imager EnMAP: Its calibration, validation, and processing chain. In: ISPRS Conference 2008, Vol. XXXVIInumber B1, International Society for Photogrammetry and Remote Sensing, pp. 1265–1270.

Storch, T., Eberle, S., Makasy, C., Maslin, S., de, A. M., Mißling, K.-D., Mühle, H., Müller, R., Engelbrecht, S., Gredel, J. and Müller, A., 2010. On the design of the ground segment for the future hyperspectral satellite mission EnMAP. In: 2010 IEEE Aerospace Conference, IEEE.